Determination of morphological characteristics of metallic nanoparticles based on modified Maxwell-Garnett fitting of optical responses

Y. Battie, A. Resano-Garcia, A. En Naciri, S. Akil, N. Chaoui

Determination of morphological characteristics of metallic nanoparticles based on modified Maxwell-Garnett fitting of optical responses

Y. Battie, A. Resano-Garcia, A. En Naciri, S. Akil, and N. Chaoui

Citation: Appl. Phys. Lett. **107**, 143104 (2015); doi: 10.1063/1.4932638
View online: http://dx.doi.org/10.1063/1.4932638
View Table of Contents: http://aip.scitation.org/toc/apl/107/14
Published by the American Institute of Physics

Determination of morphological characteristics of metallic nanoparticles based on modified Maxwell-Garnett fitting of optical responses

Y. Battie,[a] A. Resano-Garcia, A. En Naciri, S. Akil, and N. Chaoui
LCP-A2MC, Institut Jean Barriol, Université de Lorraine, 1 Bd Arago, 57070 Metz, France

(Received 21 July 2015; accepted 26 September 2015; published online 6 October 2015)

A modified effective medium theory (MEMT) is introduced to determine morphological characteristics and the volume fraction of colloidal metallic nanoparticles. By analyzing the optical absorption spectra of gold nanoparticles (NPs), this model is used to determine the distribution of prolate and oblate NPs and to demonstrate the presence of spherical NPs. In addition to interband transition, the model takes into account the longitudinal and transversal surface plasmon resonances. The results predicted by the MEMT theory were found to be in very good agreement with the shape distributions obtained by transmission electron microscopy. We found that fitting optical absorption spectra using MEMT provides a robust tool for measuring the shape and concentration of metallic NPs. © *2015 AIP Publishing LLC*. [http://dx.doi.org/10.1063/1.4932638]

Metallic nanoparticles (NPs) have promising potentials for communications, photovoltaic devices,[1] or white light processing.[2] These NPs exhibit unique optical properties such as strong surface plasmon resonances (SPRs) coming from the collective oscillations of their conduction electrons.[3] The SPR characteristics mainly depend on the nanoparticle shape.[4] As an example, silver or gold nanorods support two plasmon modes, which can be easily tuned by adjusting their aspect ratio, i.e., the ratio between the minor and the major axes of NPs.[5,6] Thus, the control of NP shape is crucial for designing nanoscale devices with uniform properties. Common bottom up elaboration processes are known to produce NPs with a shape distribution which induces drastic changes in the optical properties of NP assembly.[6–8] This inhomogeneity is mainly characterised by transmission electron microscopy (TEM). However, TEM is a time consuming local characterisation tool which only gives a two dimensional projection of 3D NPs. Moreover, electron tomography[9] is currently not implemented in conventional TEM. These limitations make crucial the development of complementary characterization tools that could accomplish *in situ* real time estimation of the NP shape distribution.

Optical absorption spectroscopy is a non-destructive optical characterisation technique, which is currently used to gain qualitative insights on nanoparticle morphology.[10–17] Several authors[11,12] have proposed to determine the size distribution of spherical metallic NPs by fitting their absorption spectra with the Mie theory.[3] However, the Mie theory fails to describe the optical properties of NP with nonspherical shape. Eustis and El-Sayed[17] have estimated the aspect ratio distribution of gold nanorods by analyzing their absorption spectra with the Gans theory. However, the authors focus their investigation on the longitudinal SPR band (L-SPR) and neglect the influence of the shape distribution on the interband transitions and the transversal plasmon band (T-SPR). Effective medium theories, which approximate the composite material as a homogeneous medium, enable the calculation of the complex effective dielectric function and require few computing resources. The Maxwell Garnett theory[18] was recently extended to describe the optical properties of spherical NPs distributed in size by averaging their polarizability. An extension of the effective medium theory was proposed by Bohren and Huffman[19] to take into account the shape distribution of spheroidal NPs. This approach was used to design broadband epsilon-near-zero composites,[20] and to interpret ellipsometric measurements performed on gold nanoisland films.[21] However, this model only considers a distribution of depolarisation factor of NPs and fails to extract directly the NP aspect ratio.

In this context, we introduce a modified effective medium theory (MEMT) which takes into account the distribution of the aspect ratio of prolate and oblate NPs. By solving the inverse problem with MEMT, we unambiguously demonstrate that the aspect ratio distribution of colloidal gold nanorods and the volume fraction of nanorods, spherical, and oblate NPs can be extracted from their optical absorption spectra.

In this letter, we consider three solutions (S1, S2, and S3) of gold NPs dispersed in water synthesised according to the seed-mediated growth method.[22] S1 was synthesized by mixing 5 ml of 5×10^{-4} M $HAuCl_4$ with a CTAB solution (5 ml, 0.2 M) and 0.6 ml of ice-cold 0.01 M $NaBH_4$. To synthesize S2 and S3, CTAB (5 ml, 0.2 M) was added to 0.20 ml and 0.25 ml of 4×10^{-3} M $AgNO_3$ solution, respectively. Then, 5.0 ml of 0.001 M $HAuCl_4$, 70 μl of 0.08 M ascorbic acid and 12 μl of S1 was added to the solution.

TEM pictures were recorded on a Phillips CM200 TEM operating at 200 kV. TEM grids were prepared by evaporating a drop of colloidal NP solution on a copper TEM grid. Note that the presence of surfactant prevents the NP aggregation. The absorption spectra of gold NP solutions were recorded in the 300–800 nm spectral range by using a Horiba Jobin-Yvon spectrophotometer equipped with a quartz cuvette of 1 mm light path. The beam diameter is 5 mm.

In the following, we consider a mixture of randomly oriented oblate and prolate NPs distributed in aspect ratio and embedded in a dielectric matrix. This nanocomposite

[a]Author to whom correspondence should be addressed. Electronic mail: yann.battie@univ-lorraine.fr

material is described by an effective dielectric function ε_{eff}. By considering the mean field approximation, the averages of the displacement $\langle \mathbf{D} \rangle$ and electric field $\langle \mathbf{E} \rangle$ can be decomposed into three contributions

$$\langle \mathbf{D} \rangle = (1-f)\varepsilon_m \langle \mathbf{E_m} \rangle + f_o \varepsilon_{np} \langle \mathbf{E_{np}}_o \rangle + f_p \varepsilon_{np} \langle \mathbf{E_{np}}_p \rangle, \quad (1)$$

$$\langle \mathbf{E} \rangle = (1-f)\langle \mathbf{E_m} \rangle + f_o \langle \mathbf{E_{np}}_o \rangle + f_p \langle \mathbf{E_{np}}_p \rangle, \quad (2)$$

where $f = f_o + f_p$ the volume fraction occupied by NPs. f_o and f_p are the volume fractions of oblate and prolate NPs, respectively. ε_{np} is the dielectric function of NPs while ε_m is the dielectric function of the surrounding medium. For gold NP diameter larger than 10 nm,[18] the intrinsic confinement can be neglected, and ε_{np} can be approximated by the bulk dielectric function.[23] $\langle \mathbf{E_m} \rangle$, $\langle \mathbf{E_{np}}_o \rangle$, and $\langle \mathbf{E_{np}}_p \rangle$ are the spatial average electric fields inside the matrix, oblate, and prolate NPs, respectively. In the quasistatic limit, i.e., for NP size smaller than the wavelength, the electric field inside NPs is defined by[19,24]

$$\langle \mathbf{E_{np}}_i \rangle = \varepsilon_m A_i \langle \mathbf{E_m} \rangle, \quad (3)$$

where i = o, p. A_i is ratio between the displacement field in the matrix and the electric field inside NPs.[19] Equation (3) assumes a homogeneous electric field inside the matrix. This approximation is still valid for a NP volume fraction smaller than 30%.[3] Indeed, for high volume fraction of NPs, the field inside the matrix becomes more and more complex and some hot spots induced by the interaction between NPs can be observed.[25,26] The effective dielectric function ε_{eff}, defined by the ratio between the spatial averages of the displacement and electric field, is calculated by combining Equations (1)–(3)

$$\varepsilon_{eff} = \varepsilon_m \frac{(1-f) + \varepsilon_{np}(f_o A_o + f_p A_p)}{(1-f) + \varepsilon_m (f_o A_o + f_p A_p)}. \quad (4)$$

The A_i coefficients are defined by[19,21]

$$A_i = \frac{1}{3} \int_0^1 P_i(r_i) \sum_{k=1}^{3} \frac{1}{\varepsilon_m + L_{ik}(r_i)(\varepsilon_{np} - \varepsilon_m)} dr_i, \quad (5)$$

where $P_o(r_o)$ and $P_p(r_p)$ are the distribution of the aspect ratio r_o and r_p of oblate and prolate NPs, respectively. $L_{i,k}$ is the depolarization parameter along each NP axis.[19] This parameter only depends on the nanoparticle shape. According to several authors,[27,28] we assume that the aspect ratio distribution can be described by a Gaussian distribution

$$P_i(r_i) = \frac{e^{-\frac{(r_i - \overline{r_i})^2}{2\sigma_i^2}}}{\int_0^1 e^{-\frac{(r_i - \overline{r_i})^2}{2\sigma_i^2}} dr_i}, \quad i = o, p, \quad (6)$$

with $\overline{r_i}$ and σ_i are the mean value and the standard deviation of the r_i distribution. The depolarization parameters of prolate $L_{p1}(r_p)$ and oblate $L_{o1}(r_o)$ NPs along their major axis only depend on the NP aspect ratio[19]

$$L_{p1}(r_p) = \frac{r_p^2}{1-r_p^2}\left(-1 + \frac{1}{2\sqrt{1-r_p^2}} \ln\left(\frac{1+\sqrt{1-r_p^2}}{1-\sqrt{1-r_p^2}}\right)\right), \quad (7)$$

$$L_{o1}(r_o) = \frac{r_o}{2(1-r_o^2)^{\frac{3}{2}}}\left(\frac{\pi}{2} - \tan^{-1}\left(\frac{r_o}{\sqrt{1-r_o^2}}\right)\right) - \frac{r_o^2}{2(1-r_o^2)}. \quad (8)$$

The depolarization parameters (L_{i2}, L_{i3}) along the other axes of NPs are deduced from the following sum rule:[19]

$$L_{i1} + L_{i2} + L_{i3} = 1, \quad (9)$$

where $L_{i1} \leq L_{i2} \leq L_{i3}$. Note that for monodispersed spherical NPs, $L_{i1} = L_{i2} = L_{i3} = 1/3$ and Equation (4) leads to the well-known Maxwell Garnett equation.[3]

In quasistatic approximation, the SPR wavelength (λ_{ri}) of metallic monodispersed NPs is given by the Fröhlich condition,[3] which occurs near the virtual pole of Equations (5)

$$0 = L_i(1-f)\varepsilon_{np}(\lambda_{ri}) + (1 - L_i(1-f))\varepsilon_m(\lambda_{ri}). \quad (10)$$

The evolution of the SPR wavelength as a function of aspect ratio of oblate and prolate gold NPs in water is illustrated in Figure 1. Due to their symmetry, prolate and oblate NPs exhibit two plasmon resonances: the transversal and the longitudinal SPR modes. For spherical NPs ($r = 1$), both plasmon modes collapse into a degenerated state. The longitudinal plasmon mode is redshifted while the transversal one is blueshifted when the aspect ratio decreases. These variations are more pronounced for prolate NPs. For wavelengths smaller than 495 nm, the optical properties of gold NPs are related to their interband transitions. Indeed, these latters damp the oscillations of conduction electrons. In other words, the SPR transversal modes of oblate and prolate NPs, which have an aspect ratio smaller than 0.67 and 0.34, respectively, are quenched (Fig. 1).

Figure 2 illustrates typical TEM images of Au NPs. It is observed that S1 NPs have a nearly spherical shape with 8.4 ± 2.4 nm mean diameter while S2 and S3 are composed of a mixture of nanorods and spherical NPs. Their diameter is two to three times larger than the S1 NPs diameter. The

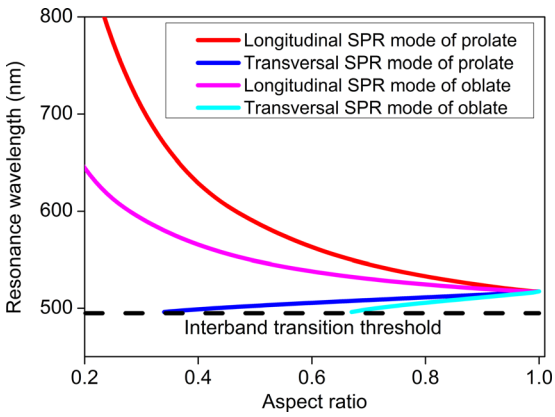

FIG. 1. Variation of the simulated SPR wavelength with the aspect ratio of prolate and oblate gold NPs dispersed in water. The NP volume fraction is 1%.

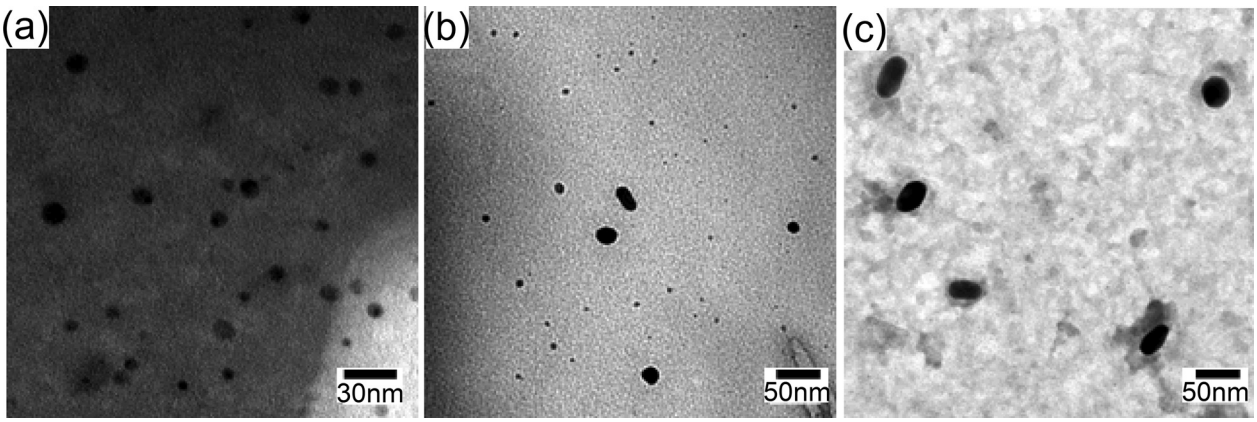

FIG. 2. TEM images of (a) S1, (b) S2 and (c) S3.

mean values of the major axis of S2 and S3 nanorods are 31 ± 6 nm and 49 ± 8 nm, respectively, while those of their minor axes are estimated to be 11 ± 3.5 nm and 26 ± 4 nm, respectively. By comparing our model with simulation based on boundary element methods (not shown), we can conclude that the quasistatic approximation can be used for nanorods length smaller than 80 nm. Indeed, the error on the aspect ratio estimation induced by retardation effect or higher order is less than 5% for NPs size smaller than 80 nm. Thus, the dimensions of the nanorods are smaller than the wavelength which permits the use of the quasistatic approximation for the interpretation of their optical properties.[3] In opposition to S3, S2 contains a larger amount of nearly spherical NPs than nanorods (Fig. 2).

The nanorods' aspect ratio distribution deduced from a TEM image analysis is reported in Fig. 3. In first approximation, and in accordance with several authors,[27,28] the former can be described by a Gaussian distribution with 0.36 ± 0.05 and 0.47 ± 0.07 mean values for S2 and S3, respectively.

The comparison between experimental and calculated optical absorption spectra of S1, S2, and S3 NPs are shown in Figure 4. The interband transition threshold of gold NPs is observed at 495 nm. Indeed, a continuous absorption corresponding to interband transitions is observed below 495 nm. The S1 absorption spectrum is characterized by a narrow band centred at 525 nm assigned to the SPR band of spherical gold NPs (Fig. 1). S2 and S3 spectra are dominated by two overlapped broad SPR bands located in the 540–560 nm and 600–670 nm spectral ranges. In opposition to S1, these bands reveal the presence of nonspherical NPs (Fig. 1). The S2 SPR band at lower energy, located at 670 nm, is redshifted by 50 nm with respect to that of S3. Contrary to S3, the S2 SPR band at lower energy has smaller amplitude than the S2 band at higher energy. The amplitude ratios between both SPR bands of S2 and S3 are close to 1.8 and 0.8, respectively.

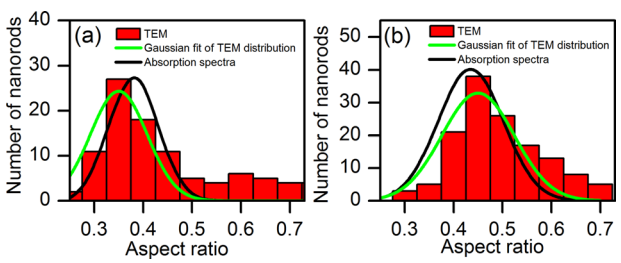

FIG. 3. Aspect ratio distribution of (a) S2 and (b) S3 nanorods estimated from TEM and optical absorption spectroscopy.

In order to improve the NP shape analysis, the measured absorption data were adjusted using the MEMT (4). The Levenberg-Marquardt algorithm was used to solve the inverse problem. Six independent parameters were considered: the volume fraction of oblate and prolate NPs, the mean aspect ratio values ($\bar{r}_o$, $\bar{r}_p$) and the standard deviations (σ_o, σ_p) of the distribution of the aspect ratio of oblate and prolate NPs. These parameters are fitting simultaneously. In other words, the fit of absorption spectra is used to extract the aspect ratio distribution of NPs. In first approximation, nanorods were assimilated to prolate NPs. The average central processing unit time needed to fit the data is estimated at 40 s. As shown in Fig. 4, a very good agreement is found between the measured and the calculated absorption spectra. The root mean square error is less than 0.1 for all samples. Contrary to S2 and S3, the fit of the S1 absorption spectra slightly deviates from the measurements. S1 mainly contains spherical NPs with a 8.4 nm mean diameter for which the intrinsic confinement can occur.[18] However, the model does not take into account this effect. The correlation matrix (not shown here) suggests that all the parameters are independent. We also check that initial input values have a negligible effect on the final solution.

The two dimensional distribution of the depolarization parameters (L_{i1}, L_{i2}) determined from the analysis of absorption spectra is reported in Fig. 5. To make easier the interpretation, the locus of prolate ($L_{1p} = 1 - 2L_{2p}$) and oblate ($L_{1o} = L_{2o}$) NPs are shown as a red and blue dashed lines, respectively. In accordance with TEM measurements (Fig. 5), S1 has a narrow (L_1, L_2) distribution centered at (1/3, 1/3), confirming that S1 is mainly composed of spherical NPs. On the contrary, (L_1, L_2) distributions of S2 and S3 reveal the presence of oblate and prolate NPs distributed in aspect ratio. The L_1 mean value of S2 and S3 oblate NPs is estimated at 0.27. This value corresponds to a 0.65 average aspect ratio of oblate NPs. However, no oblate NPs can be observed on the TEM images because these latters only provides a two dimensional projection of NPs. This can be explained by the fact that the minor axis of oblate NPs are oriented along the normal of the TEM grid in order to maximize their contact with

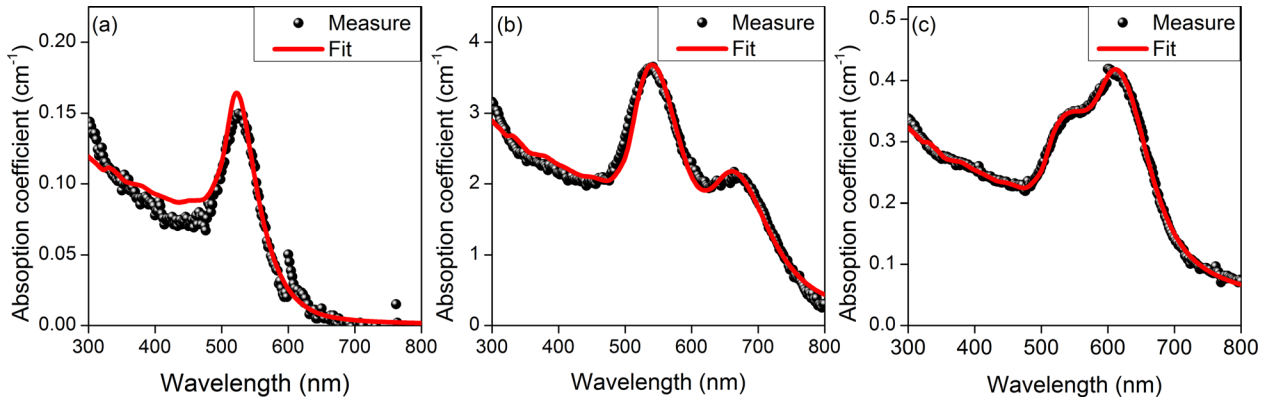

FIG. 4. Measured (black dot) and calculated (red solid line) absorption spectra of (a) S1, (b) S2, and (c) S3.

the grid surface.[29] This suggests that the NPs in S2 and S3, which seems to have a spherical shape in TEM images, are probably slightly flattened along the normal of the TEM grid.[29] According to the Fröhlich condition[3] (10) (Fig. 1) and the (L_1, L_2) distribution (Fig. 5), the band located in the 545–560 nm and 610–665 nm regions can be assigned to the longitudinal plasmon mode of oblate and prolate NPs, respectively (Fig. 1). The energies of the transversal SPR mode of S2 and S3 NPs, calculated from the Fröhlich condition (10), are larger or in the same order of magnitude than the interband transition threshold. In other words, the transversal plasmon mode of S2 and S3 NPs is damped by the interband transitions. In accordance with the amplitude of SPR bands, the volume fraction of S2 oblate NPs ($f_o = 3.4 \times 10^{-4} \pm 1 \times 10^{-5}$%) is 5 times larger than that of the prolate ($f_p = 6.2 \times 10^{-5} \pm 1 \times 10^{-5}$%). On the other hand, S3 contains a slightly smaller amount of oblate NPs than prolate NPs ($f_o = 2.7 \times 10^{-5} \pm 1 \times 10^{-6}$%, $f_p = 2.0 \times 10^{-5} \pm 1 \times 10^{-6}$%). TEM measurements enables the determination of the ratio between the volumes occupied by oblate and prolate NPs. Note that the aspect ratio of prolate nanoparticles deduced from the fit of optical measurement is taken into account to calculate the volume of oblate nanoparticles. These ratios, measured over more than 200 NPs, were found to be 4.3 and 0.8 for S2 and S3, respectively. These values are close to those obtained from the optical data analysis. The deviations can be attributed to the low number of NPs probed in TEM. Moreover, the accuracy the NP radius measured by TEM is highly dependant to the TEM calibration, the charging effect which can degrade the image quality, the presence of NP aggregates, and the failure of TEM to resolve NPs smaller than few nanometres.

To validate the proposed method, the aspect ratio distributions of S2 and S3 prolate NPs deduced from absorption spectroscopy were compared to those measured from TEM (Fig. 3). Both techniques give similar distributions confirming the correctness of our procedure. The deviation between the mean value of aspect ratio obtained by TEM and absorption spectroscopy is smaller than 7%. Unlike TEM measurements, our procedure enables the extraction of the prolate and oblate volume fraction. The volume of the solution probed by the light beam is 20 mm^3. By considering the NP volume fraction and the mean volume of NPs extracted from absorption and TEM measurements, we can conclude that the distribution of aspect ratio is recorded over 10^{10}–10^{11} NPs. Moreover, optical absorption spectroscopy is non-local, non-destructive, and is compatible with *in situ* and real time

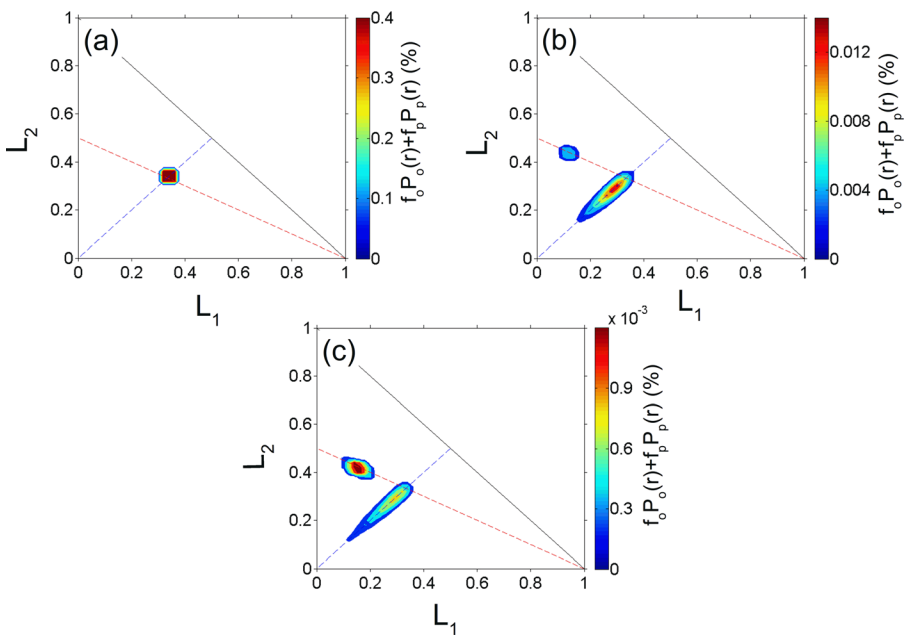

FIG. 5. (L_1, L_2) volume fraction distribution of (a) S1, (b) S2, and (c) S3. The prolate axis (red dashed line) and oblate axis (blue dashed line) are also reported.

measurements. In other words, the analysis of the optical properties through MEMT offers an attractive alternative to TEM measurements for the determination of the aspect ratio distribution of a colloid.

In summary, we have introduced an effective medium theory, which takes into account the aspect ratio distribution of oblate and prolate NPs. This theory has been used to quantitatively analyze the absorption spectra of gold NPs. This approach can also be used for other NPs such as silver, copper, or metallic alloy NPs, which present shape sensitive plasmon resonances. As we have previously reported,[24] the distribution of depolarization parameters of complex NP shape can also be estimated from absorption spectra. To avoid inaccurate characterization and to respect the limitations set by the model, the NP size must be higher than 10 nm but smaller than 80 nm and their concentration must be smaller than 30%. We demonstrated that optical absorption spectroscopy provides a robust and straightforward tool for measuring the shape and concentration of metallic NPs. This can be useful for a quick determination of the aspect ratio distribution of prolate and oblate NPs. Furthermore, the number of probed NPs using optical absorption spectroscopy is much larger than that using TEM which is still a local measurement technique and which results are highly influenced by the sample preparation.

[1]D. Derkacs, S. H. Lim, P. Matheu, W. Mar, and E. T. Yu, Appl. Phys. Lett. **89**, 93103 (2006).
[2]R. Kitsomboonloha, C. Ngambenjawong, W. S. Mohammed, M. B. Chaudhari, G. L. Hornyak, and J. Dutta, Micro Nano Lett. **6**, 342 (2011).
[3]U. Kreibig and M. Vollmer, *Optical Properties of Metal Clusters* (Springer, Berlin, 1995).
[4]C. Noguez, J. Phys. Chem. C **111**, 3806 (2007).
[5]O. L. Muskens, G. Bachelier, N. D. Fatti, F. Vallee, A. Brioude, X. Jiang, and M. P. Pileni, J. Phys. Chem. C **112**, 8917 (2008).
[6]R. Sayah, L. Nadar, F. Vocanson, Y. Battie, S. Reynaud, R. Vera, A. Boukenter, and N. Destouches, Microporous Mesoporous Mater. **139**, 45 (2011).
[7]Y. Battie, N. Destouches, F. Chassagneux, D. Jamon, L. Bois, N. Moncoffre, and N. Toulhoat, Opt. Mater. Express **1**, 1019 (2011).
[8]L. Qiu, T. A. Larson, D. Smith, E. Vitkin, M. D. Modell, B. A. Korgel, V. Konstantin Sokolov, E. B. Hanlon, I. Itzkan, and L. T. Perelman, Appl. Phys. Lett. **93**, 153106 (2008).
[9]J. R. Jinschek, K. J. Batenburg, H. A. Calderon, R. Kilaas, V. Radmilovic, and C. Kisielowski, Ultramicroscopy **108**, 589 (2008).
[10]Z. J. Hu, S. Hou, Y. L. Ji, T. Wen, W. Q. Liu, H. Zhang, X. W. Shi, J. Yan, and X. C. Wu, AIP Adv. **4**, 117137 (2014).
[11]V. Amendola and M. Meneghetti, J. Phys. Chem. C **113**, 4277 (2009).
[12]F. Bourquard, A. S. Loir, C. Donnet, and F. Garrelie, Appl. Phys. Lett. **104**, 104101 (2014).
[13]C. Jing, Z. Gu, Y.-L. Ying, D.-W. Li, L. Zhang, and Y.-T. Long, Anal. Chem. **84**, 4284 (2012).
[14]W. Haiss, N. T. K. Thanh, J. Aveyard, and D. G. Fernig, Anal. Chem. **79**, 4215 (2007).
[15]N. G. Khlebtsov, Anal. Chem. **80**, 6620 (2008).
[16]K. Slyusarenko, B. Abécassis, P. Davidson, and D. Constantin, Nanoscale **6**, 13527 (2014).
[17]S. Eustis and M. A. El-Sayed, J. Appl. Phys. **100**, 044324 (2006).
[18]Y. Battie, A. Resano-Garcia, N. Chaoui, Y. Zhang, and A. En Naciri, J. Chem. Phys. **140**, 044705 (2014).
[19]C. F. Bohren and D. R. Huffman, *Absorption and Scattering by a Sphere, in Absorption and Scattering of Light by Small Particles* (Wiley, Germany, 1998).
[20]A. V. Goncharenko and A. O. Pinchuk, Opt. Mater. Express **4**, 1276 (2014).
[21]Y. Battie, A. En Naciri, W. Chamorro, and D. Horwat, J. Phys. Chem. C **118**, 4899 (2014).
[22]B. Nikoobakht and M. A. El-Sayed, Chem. Mater. **15**, 1957 (2003).
[23]E. D. Palik, *Handbook of Optical Constants of Solids* (Academic press, Boston, 1998).
[24]A. Resano-Garcia, Y. Battie, A. E. Naciri, S. Akil, and N. Chaoui, J. Chem. Phys. **142**, 134108 (2015).
[25]S. Enoch, R. Quidant, and G. Badenes, Opt. Express **12**, 3422 (2004).
[26]S. Ducourtieux, V. A. Podolskiy, S. Gresillon, S. Buil, B. Berini, P. Gadenne, A. C. Boccara, J. C. Rivoal, W. A. Bragg, K. Banerjee, V. P. Safonov, V. P. Drachev, Z. C. Ying, A. K. Sarychev, and V. M. Shalaev, Phys. Rev. B **64**, 165403 (2001).
[27]N. Xu, B. Bai, Q. Tan, and G. Jin, Opt. Express **21**, 2987 (2013).
[28]F. J. Recio, N. Zabala, A. Rivacoba, P. Crespo, A. Ayuela, P. M. Echenique, and A. Hernando, J. Phys. Chem. C **119**, 7856 (2015).
[29]K. R. Brown, D. G. Walter, and M. J. Natan, Chem. Mater. **12**, 306 (2000).